

1  
2  
3  
4  
5  
6  
7  
8  
9  
10  
11  
12  
13  
14  
15  
16  
17  
18  
19  
20  
21  
22

**Detection of small drizzle droplets in a large cloud chamber using  
ultra high-resolution radar**

Zeen Zhu<sup>1</sup>, Fan Yang<sup>1</sup>, Pavlos Kollias<sup>1,2</sup>, Raymond A. Shaw<sup>3</sup>, Alex B. Kostinski<sup>3</sup>, Steve  
Krueger<sup>4</sup>, Katia Lamer<sup>1</sup>, Nithin Allwayin<sup>3</sup>, Mariko Oue<sup>2</sup>

<sup>1</sup>Brookhaven National Laboratory, Upton, NY, USA

<sup>2</sup>Stony Brook University, Stony Brook, NY, USA

<sup>3</sup>Michigan Technological University, Houghton, MI, USA

<sup>4</sup>University of Utah, Salt Lake City, UT, USA

Corresponding author: Zeen Zhu (zzhu1@bnl.gov)

23 **Abstract**

24

25 A large convection cloud chamber has the potential to produce drizzle-sized droplets, thus offering  
26 a new opportunity to investigate aerosol-cloud-drizzle interactions at a fundamental level under  
27 controlled environmental conditions. One key measurement requirement is the development of  
28 methods to detect the low concentration drizzle drops in such a large cloud chamber. In particular,  
29 remote sensing methods may overcome some limitations of in situ methods.

30

31 Here, the potential of an ultra-high-resolution radar to detect the radar return signal of a small  
32 drizzle droplet against the cloud droplet background signal is investigated. It is found that using a  
33 small sampling volume is critical to drizzle detection in a cloud chamber to allow a drizzle drop in  
34 the radar sampling volume to dominate over the background cloud droplets signal. For instance, a  
35 radar volume of 1 cubic centimeter ( $cm^3$ ) would enable the detection of drizzle embryos with  
36 diameter larger than  $40 \mu m$ . However, the probability of drizzle sampling also decreases as the  
37 sample volume reduces, leading to a longer observation time. Thus, the selection of radar volume  
38 should consider both of the signal power and the drizzle occurrence probability. Finally,  
39 observations from the Pi Convection-Cloud Chamber are used to demonstrate the single drizzle  
40 particle detection concept using small radar volume. The results presented in this study also  
41 suggest new applications of ultra-high-resolution cloud radar for atmospheric sensing.

42

43

44

45

46

47

48

49

50

51

## 52        **1. Introduction**

53        Drizzle formation is one of the most important microphysical processes in warm clouds. Yet the  
54        processes controlling drizzle formation remain poorly understood (Wood, 2012). The most  
55        challenging aspect is the initial formation of drizzle embryos with diameter around  $30 \mu\text{m} \sim 50$   
56         $\mu\text{m}$ . The formation of small drizzle particles in this range can neither be adequately explained by  
57        the traditionally-defined condensation growth process nor by the traditionally-defined collision-  
58        coalescence (C-C) process owing to their low efficiency (Yau and Rogers, 1996; Pruppacher and  
59        Klett, 2012; Falkovich et al., 2006; Beard and Ochs III, 1993). Several mechanisms have been  
60        hypothesized to explain the efficiency of these processes including i) fine-scale turbulence in cloud  
61        (Pinsky and Khain, 1997; Shaw, 2003); ii) giant cloud condensation nuclei (GCCN) (Johnson,  
62        1982; Feingold et al., 1999); and iii) longwave cooling (Roach, 1976; Harrington et al., 2000).  
63        Nevertheless, it remains unclear to which extent these proposed mechanisms can adequately  
64        explain the origin of drizzle embryos.

65        One main barrier that hinders our ability to investigate the drizzle initiation process is the lack of  
66        observations with sufficient sensitivity and spatiotemporal resolution to detect the early growth of  
67        drizzle particles. As such an instrumented large convection cloud chamber with well-controlled  
68        initial and boundary conditions might help to improve our understanding of the drizzle initiation  
69        mechanism (Shaw et al., 2020). Unlike other types of chambers, a convection-cloud chamber can  
70        generate a steady state cloud system for hours in a turbulent environment by maintaining a warm  
71        saturated bottom surface, a cold saturated top surface, and a constant aerosol injection rate (Chang  
72        et al., 2016). The Michigan Tech Pi convection chamber with a dimension of 2 m x 2 m x 1 m  
73        (width x depth x height) has been used to explore aerosol-cloud-turbulence interactions, however,  
74        the Pi Chamber is too small to initiate drizzle embryos mainly due to the relatively short lifetime  
75        of cloud droplets therein. Results from large eddy simulations indicate that drizzle can be initiated  
76        in a large convection-cloud chamber with a height on the order of 10 m (Thomas et al., 2023).  
77        However, the drizzle drops are sparse in a large chamber, so the detection of single drizzle embryos  
78        in a large cloud chamber is challenging for in-situ probes that generally have a sampling volume  
79        of only a few cubic centimeters. On the other hand, active remote sensors have the ability to rapidly  
80        sample large volumes and thus offer an attractive option for the detection of small drizzle droplets  
81        in a cloud chamber.

82

83 Here, we will demonstrate that the detection of an individual drizzle droplet in the presence of  
84 numerous cloud droplets is possible with a radar that can achieve a very small sampling volume.

85 The detection of individual drizzle droplets is possible because the radar signal-to-noise ratio (SNR)  
86 of a point target (drizzle droplet) is not affected by the radar observational volume, while the SNR  
87 of a distributed target (cloud droplets) scales with the radar volume. In the following sections, the  
88 detection limits of an individual drizzle particle are investigated using idealized particle size  
89 distributions and real particle size distributions from the Michigan Tech Pi Chamber. In the end,  
90 the potential of THz radars offering unprecedented sub-centimeter range resolution will be  
91 discussed for developing the single drizzle detection radar (Cooper and Chattopadhyay, 2014).

92

93

94

## 95 **2. Drizzle detection using radar**

96

97 The detection of early drizzle particles in clouds has been the topic of extensive research. First, the  
98 radar needs to have sufficient sensitivity to detect cloud and drizzle droplets. This is typically  
99 accomplished using millimeter-wavelength radar (Kollias et al., 2007). Early methodologies for  
100 the detection of drizzle drop in clouds employ the use of reflectivity thresholds, ranging  
101 from  $-15$  to  $-20$  dBZ, to identify drizzle existence (Frisch et al., 1995; Liu et al., 2008; Comstock  
102 et al., 2004). Kollias et al. (2011) introduced the use of the radar Doppler spectra skewness as a  
103 more sensitive method for detecting the presence of small drizzle droplets (Acquistapace et al.,  
104 2017; Zhu et al., 2022). The radar Doppler spectra technique improved the detection of drizzle  
105 droplets that can produce as low as  $-30$  dBZ (Zhu et al., 2022).

106

107 However, the use of the radar Doppler spectra technique in a cloud chamber is challenging. First,  
108 this will require that the radar point vertically to take advantage of the differential velocity between  
109 cloud and drizzle droplets. If we assume a monodisperse droplet size distribution (DSD) and  
110 Rayleigh scattering conditions, a drizzle detection limit of  $-30$  dBZ is equivalent to a concentration  
111 of  $10^{-3} \text{ cm}^{-3}$  of drizzle droplets with diameter equal to  $100 \mu\text{m}$  or a concentration of  $6.4 \times 10^{-2}$   
112  $\text{cm}^{-3}$  of drizzle droplets with  $50 \mu\text{m}$  diameter. In the former case, the drizzle particle size is quite

113 large and not quite an early drizzle droplet detection. In the latter case, the concentration of drizzle  
 114 droplets is much higher than the concentration observed in nature ( $\sim 10^{-4} \text{ cm}^{-3}$ ) (Zhu et al., 2022).  
 115 Furthermore, the conventional cloud radar has range resolution of tens of meters, which is not  
 116 applicable in a chamber facility which may be on the order of several meters (approaching the  
 117 collision mean free path).

118  
 119 As a result, we consider alternative methods to increase the probability of early drizzle droplet  
 120 detection against the cloud droplet signal. As the number concentration of drizzle particle is low,  
 121 by applying a small radar sampling volume  $V_{Radar}$ , it is possible that only one drizzle droplet is  
 122 present in  $V_{Radar}$ . In this case, the drizzle particle can be considered as a point target with  
 123 backscattering cross section  $\sigma(m^2)$  and the received radar echo power  $P_r$  (mW) is commonly  
 124 expressed as (Battan, 1973):

$$126 \quad P_{r,drizzle} = P_t \frac{G^2 \lambda^2}{(4\pi)^3 r^4} \sigma(D_d) \quad (1)$$

127  
 128 where  $P_t$  is the transmit peak power (mW),  $G$  is the antenna gain,  $r$  (m) is the range of the target  
 129 relative to the radar receiver and  $\lambda$  (m) is the radar wavelength. It is noteworthy that  $P_r$  for a point  
 130 target does not depend on the radar sampling volume  $V_{Radar}$ . For distributed targets such as a cloud  
 131 droplet population described by a droplet size distribution (DSD) that represents the number  
 132 concentration of cloud droplets as a function of diameter, the received radar echo power is given  
 133 by:

$$135 \quad P_{r,cloud} = P_t \frac{G^2 \lambda^2}{(4\pi)^3 r^4} \cdot V_{Radar} \cdot \sum_{i=0}^n N_c(D_i) \sigma(D_i) \Delta D_i \quad (2)$$

136  
 137 Where  $n$  is the number of cloud droplets in the radar volume and  $N_c(D)$  is the DSD with units of  
 138  $m^{-4}$ . In this case, the received radar echo power depends on the radar sampling volume, which is  
 139 given by the following expression:

$$140 \quad V_{Radar} = \pi \left( \frac{r \theta_{3dB}}{2} \right)^2 \cdot \Delta R \quad (3)$$

141

142 where  $\theta_{3dB}$  is antenna radiation pattern 3-dB beamwidth in radians and  $\Delta R$  is the range resolution.

143 Assuming Rayleigh scattering, the backscatter cross section of the drizzle and cloud droplets is

144 proportional to the sixth power of the particle diameter and inversely proportional to the fourth

145 power of the wavelength ( $\sigma(D) \sim D^6/\lambda^4$ ). Combing Eq. 1 and Eq. 2, the ratio of radar received

146 echo power from drizzle and cloud is given by the following expression:

147

$$\frac{Signal}{Background} = \frac{P_{r,drizzle}}{P_{r,cloud}} = \frac{1}{V_{Radar}} \cdot \frac{D_d^6}{\sum_{i=0}^n N_c(D_i) D_i^6 \Delta D_i}. \quad (4)$$

149

150 Eq. 4 indicates that the probability of detecting a single drizzle droplet in the radar sampling

151 volume increases inversely to the radar sampling volume (point vs distributed target).

152

### 153 3. Detection requirement

154

155 Here, we will evaluate how small the radar sampling volume needs to be to detect drizzle drops

156 with different diameters against three background (cloud) conditions: i) monodisperse cloud DSD,

157 ii) cloud DSD from a theoretical model and iii) observed cloud DSD from the Michigan Tech Pi

158 Chamber. For simplicity, we will assume that a drizzle drop is detectable if its radar return power

159 is equal to that of the background echo contributed from cloud droplets.

160

#### 161 3.1. Monodisperse cloud DSD

162

163 We first construct an idealized scenario by considering two categories of droplets, i.e. cloud droplet

164 with a diameter of  $D_c$  and a single drizzle drop with a diameter of  $D_d$ , the number concentration

165 of cloud droplets in the radar sampling volume is  $N_c$  ( $m^{-3}$ ).

166

167 In this case, Eq. 4 is simplified as:

168

169

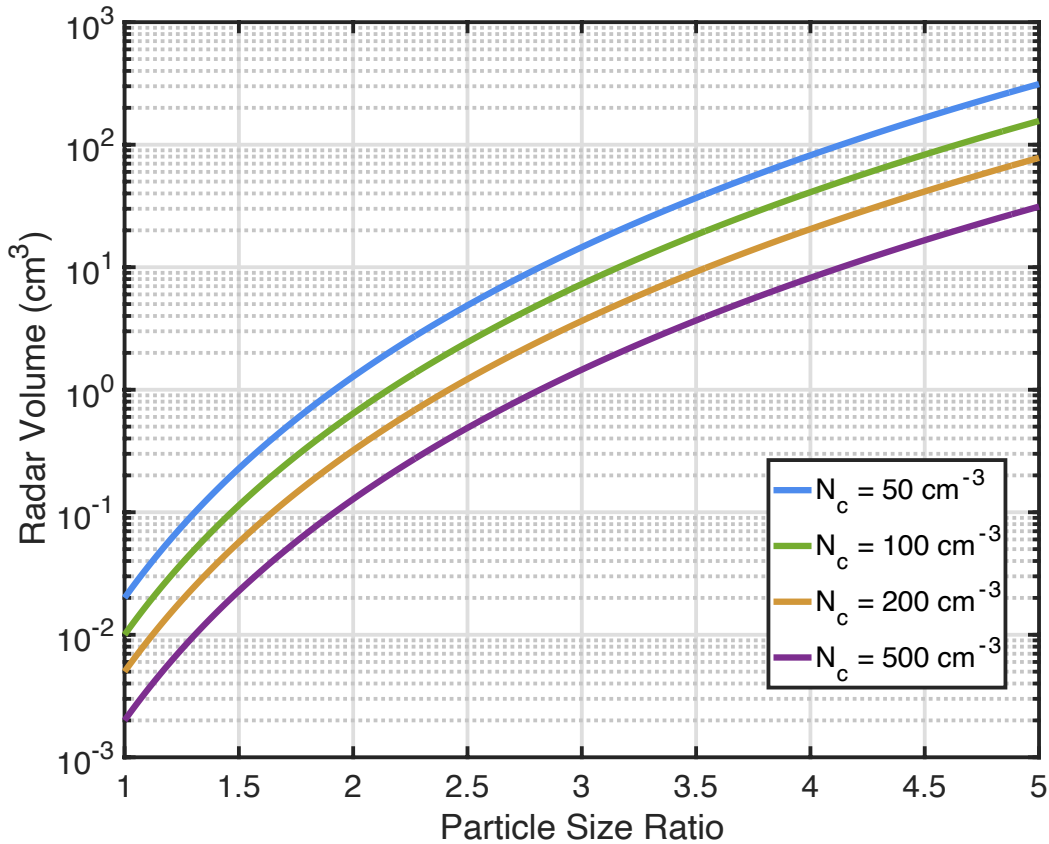
170

$$\frac{Signal}{Background} = \frac{1}{V_{Radar}} \cdot \frac{D_d^6}{N_c \cdot D_c^6} \quad (5)$$

171

172 When the signal power equals to the background, the radar sampling volume enabling single  
 173 drizzle particle detection is estimated as a function of the size ratio  $x = \frac{D_d}{D_c}$  shown in Fig. 1. The  
 174 results are shown for various cloud droplet concentrations. It is noted that the required radar  
 175 volume for detection depends on the drizzle drop size and the cloud number concentration. Larger  
 176 radar volume would be required for drizzle detection as the particle size ratio increase; for a given  
 177 particle size ratio, decreasing cloud number concentration can enhance the required radar volume.  
 178 For example, if the cloud number concentration is  $50 \text{ cm}^{-3}$  and the mean cloud diameter ( $D_c$ ) is  
 179  $20 \mu\text{m}$ , then the detection of a drizzle particle with diameter of  $40 \mu\text{m}$  ( $x = 2$ ) requires radar  
 180 volume around  $1 \text{ cm}^3$ . Such sampling volume are not achievable with traditional radar systems  
 181 that employ sampling volumes of the order of  $1000 \text{ m}^3$  or more (Kollias et al., 2016).

182



183

184 Figure 1: Radar observational volume for single-drizzle-drop detection as a function of particle  
 185 size ratio  $x = \frac{D_d}{D_c}$ . Lines of different color represent clouds number concentration ( $N_c$ ):  $50 \text{ cm}^{-3}$   
 186 (blue),  $100 \text{ cm}^{-3}$  (green),  $200 \text{ cm}^{-3}$  (yellow) and  $500 \text{ cm}^{-3}$  (purple).

187

188

### 189 3.2 Drizzle detection against an idealized cloud droplet background

190

191 In a realistic cloud chamber environment, we expect a population of cloud droplets with various  
 192 sizes that can be represented by a DSD. Particularly, when condensation and fallout are the main  
 193 sources and sinks for the evolution equation for the DSD, the DSD in the cloud chamber can be  
 194 approximately described by theoretically derived distributions (Saito et al., 2019; Chandrakar et al.,  
 195 2020; Krueger, 2020). Here we adapt the theoretical DSD formula derived by Krueger (2020) to  
 196 investigate the ability of a radar to detect a drizzle embryo present in a small sample volume under  
 197 different chamber environment conditions. To better represent the cloud DSD under different  
 198 environments, the analytical DSD is rearranged to be expressed as a function of liquid water  
 199 content ( $LWC_c$ ;  $g \text{ m}^{-3}$ ) and number concentration ( $N_c$ ;  $m^{-3}$ ) as:

200

$$201 \quad N(D_c) = \frac{2N_c D_c}{\pi^{1/2}} \left( \frac{4\Gamma\left(\frac{5}{4}\right) \pi^{1/2} \rho_l N_c}{3LWC_c} \right)^{2/3} \exp \left( - \left( \frac{4\Gamma\left(\frac{5}{4}\right) \pi^{1/2} \rho_l N_c}{3LWC_c} \right)^{\frac{4}{3}} \left( \frac{D_c}{2} \right)^4 \right) \quad (6)$$

202

203 where  $\rho_l$  is liquid water density ( $g \text{ m}^{-3}$ ), and  $D_c$  is cloud droplet diameter ( $m$ ).  $N(D_c)$  represents  
 204 the number concentration of cloud droplet for the given diameter ( $cm^{-3} \mu m^{-1}$ ).

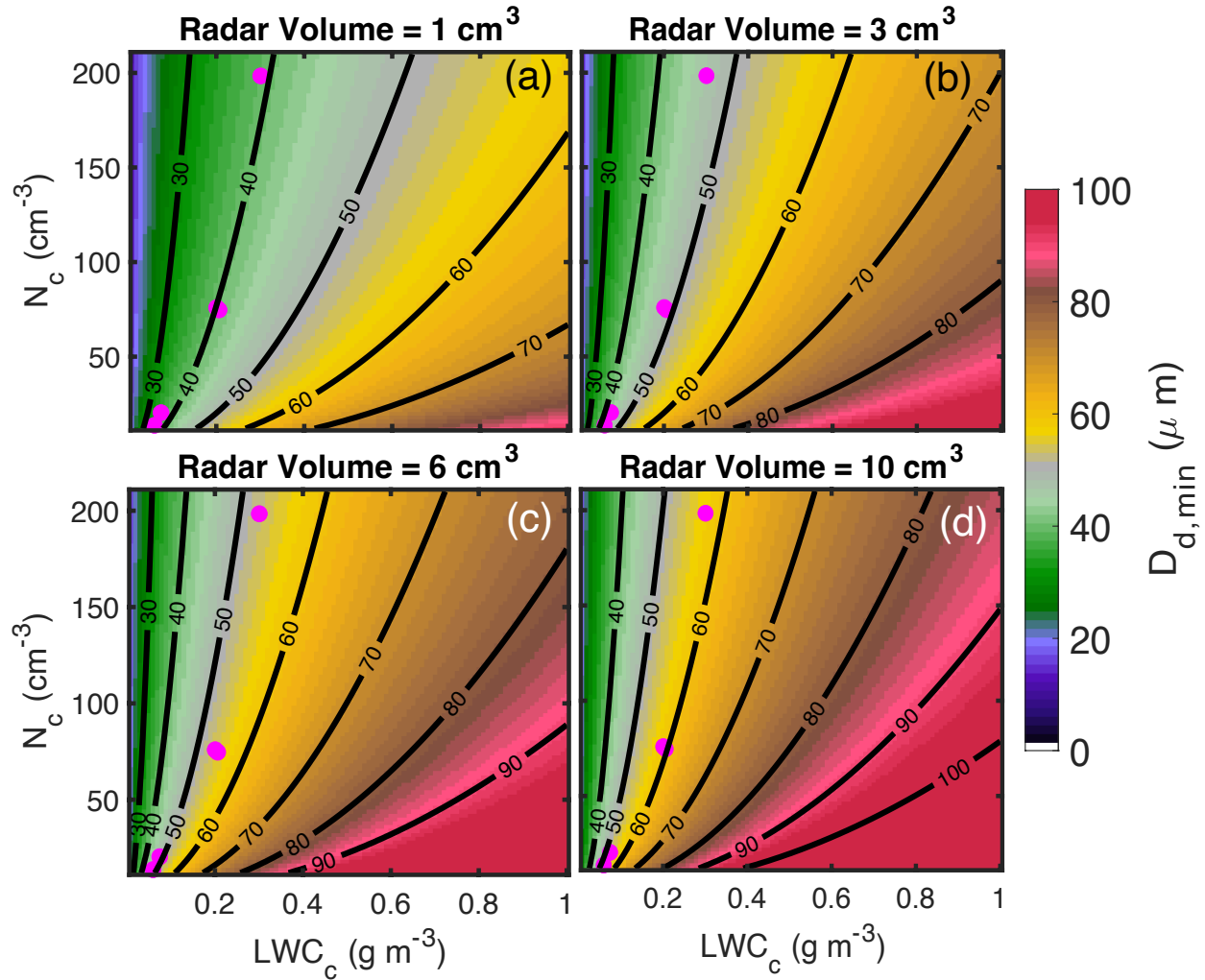
205

206 Here we define the minimal drizzle drop ( $D_{d,min}$ ) as the size of particle with radar return power  
 207 equal to the total return power from cloud droplets in a given radar volume ( $V$ ). Given the cloud  
 208 DSD described by Eq. 6,  $D_{d,min}$  can be estimated as:

209

$$210 \quad D_{d,min}^6 = \int V N(D_c) D_c^6 dD \quad (7)$$





211

212 Figure2: The minimal detectable drizzle particle ( $D_{d,min}$ ) under different  $LWC_c$  and  $N_c$  conditions  
 213 with radar sampling volume of (a)  $1\text{ cm}^3$ , (b)  $3\text{ cm}^3$ , (c)  $6\text{ cm}^3$  and (d)  $10\text{ cm}^3$ . The black lines are  
 214 the  $D_{d,min}$  contour of  $30\text{ }\mu\text{m}$ ,  $40\text{ }\mu\text{m}$ ,  $50\text{ }\mu\text{m}$ ,  $60\text{ }\mu\text{m}$ ,  $70\text{ }\mu\text{m}$ . The magenta dots indicate the  $LWC_c$   
 215 and  $N_c$  observed in the Pi-cloud chamber.

216

217 Fig. 2 illustrates  $D_{d,min}$  under different  $LWC_c$  and  $N_c$  combinations for various radar volumes. For  
 218 a given steady-state cloud in a convection chamber (i.e., fixed  $LWC_c$  and  $N_c$ ),  $D_{d,min}$  generally  
 219 increases as the radar volume increases. This is because larger radar volumes contain more cloud  
 220 droplets that produce stronger background power, thus only a larger drizzle particle with a higher  
 221 backscattering signal would be detectable. On the other hand, for a given radar observational  
 222 volume,  $D_{d,min}$  is jointly determined by  $LWC_c$  and  $N_c$  which are inversely proportional. As such,

223  $D_{d,min}$  increases rapidly with increasing  $LWC_c$  but slightly decreases with increasing  $N_c$ . This  
 224 contrasting relationship is caused by a larger sensitivity of radar reflectivity to particle size than to  
 225 number concentration. Thus, increasing  $LWC_c$  can increase mean cloud particle size and greatly  
 226 enhance the background power, leading to a larger detectable  $D_{d,min}$ . On the other side, when  
 227  $LWC_c$  is fixed, increasing cloud total number concentration tends to decrease particle size. The  
 228 reduced cloud particle size would reduce the backscattering power and more than compensate for  
 229 the power enhancement contributed from the increased number concentration.

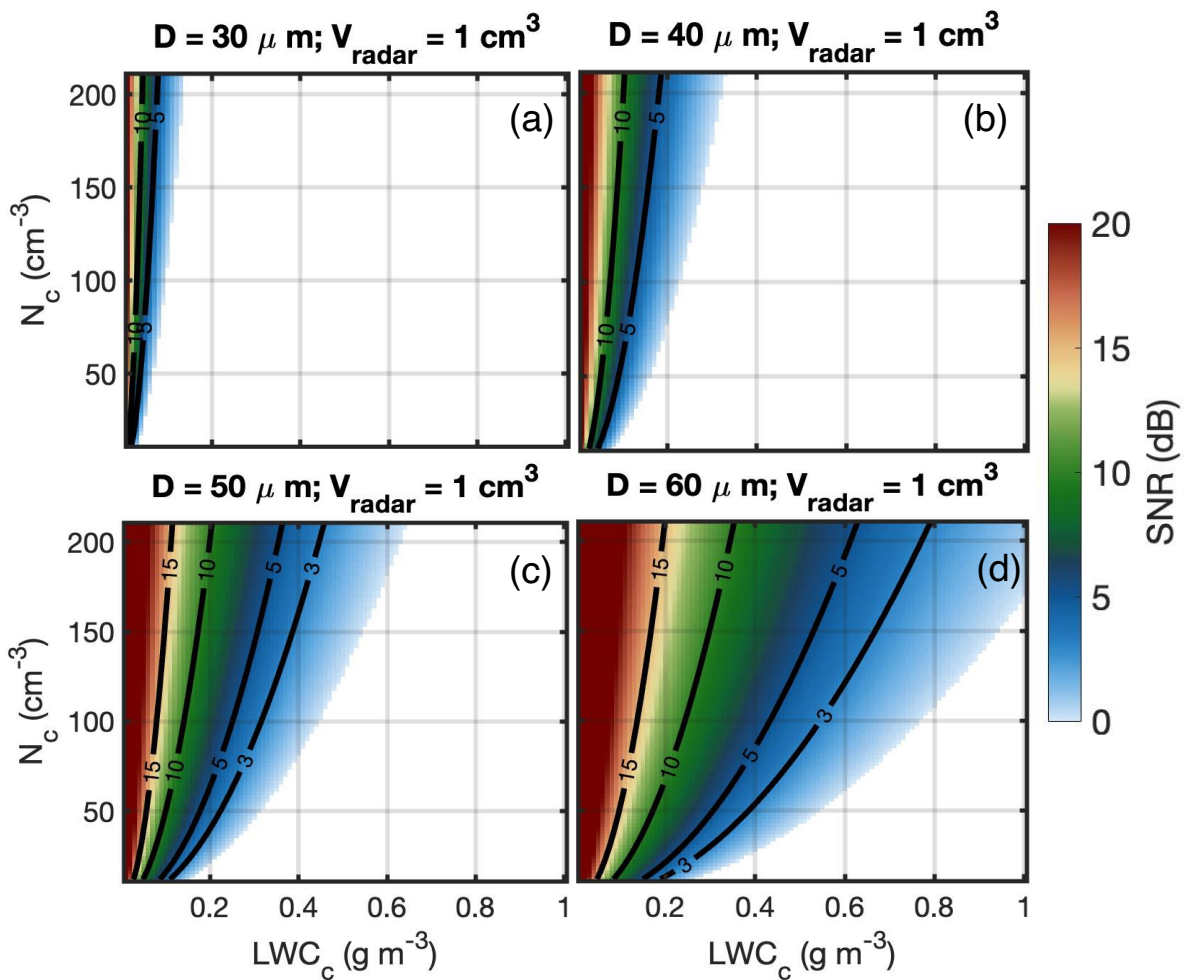
230  
 231 It should be noted that  $LWC_c$  and  $N_c$  in a convection cloud chamber have a stronger correlation  
 232 compared with those in atmospheric clouds (Shaw et al., 2023). Instead, the  $LWC_c$  and  $N_c$  often  
 233 exhibit a positive covariance relationship. To understand the typical value of these two quantities  
 234 in the chamber environment, we refer to typical measurement data from the Pi Chamber (magenta  
 235 dots in Fig. 2). The data are from experiments conducted by Chandrakar et al. (2018). We can  
 236 notice that for this specific experiment set up, drizzle embryos with diameter ranging from  $40 \mu m$   
 237 to  $60 \mu m$  can be detected using radar observational volume from  $1 cm^3$  to  $10 cm^3$ .

238  
 239 The aforementioned estimation is conducted under the assumption that signal (drizzle) power is  
 240 equal to the background (cloud) power. In practice, to reduce the detection false alarms, the drizzle  
 241 signal should be larger than the backgrounds. Here we define the signal to noise ratio (SNR) to  
 242 investigate the drizzle detectability in the chamber environment:

243  
 244 
$$SNR = 10 \log_{10} \left( \frac{D_d^6}{\int VP(D_c) D_c^6 dD} \right). \quad (8)$$

245  
 246 Fig. 3 shows the estimated SNR for four drizzle particles under varying  $LWC_c$  and  $N_c$  conditions  
 247 with a radar volume of  $1 cm^3$ . Generally, a smaller  $LWC_c$  and a larger  $N_c$  correspond to a large  
 248 SNR, which is preferable for drizzle detection. If we arbitrarily choose  $SNR > 3$  as the detection  
 249 threshold, to detect a drizzle drop with diameter of  $50 \mu m$  in a radar volume of  $1 cm^3$  (Fig. 3c),  
 250  $LWC_c$  in the cloud chamber should be lower than  $0.3 g m^{-3}$  and  $N_c$  should be high than  $90 cm^{-3}$ .  
 251 The required  $LWC_c$  and  $N_c$  would be different for different drizzle particle targets: to detect drops  
 252 with diameter of  $60 \mu m$ ,  $LWC_c$  should be lower than  $0.5 g m^{-3}$  and  $N_c$  should be higher than 90

253  $cm^{-3}$ . It should be noted that although a drizzle drop is more likely to be detected by the radar at a  
 254 lower  $LWC_c$ , drizzle initiation is generally more likely to occur at a higher  $LWC_c$  because the  
 255 collision-coalescence rate is thought to be proportional to the square of  $LWC$  (Kostinski and Shaw,  
 256 2005). This suggests appropriate  $LWC_c$  and  $N_c$  combinations should be achieved such that drizzle  
 257 can form by the C-C process in a convection cloud chamber and it can also be detected by radar in  
 258 a small sampling volume. It is also noted that the results shown in Fig.3 are based on a radar  
 259 volume of  $1\text{ cm}^3$ , and the estimated  $SNR$  would change if a different radar volume size is applied.  
 260 For instance, increasing the radar volume will enhance the background power thus decreasing the  
 261  $SNR$  for the given cloud chamber environment.



262  
 263 Figure 3: SNR of the drizzle signal under different  $LWC$  and  $N$  conditions in a  $1\text{ cm}^3$  radar sample  
 264 volume for drizzle diameters of  $30\text{ }\mu\text{m}$ ,  $40\text{ }\mu\text{m}$ ,  $50\text{ }\mu\text{m}$ ,  $60\text{ }\mu\text{m}$ . The black lines are SNR contours  
 265 of 3 dB, 5 dB, 10 dB and 15 dB. SNR lower than 0 is indicated as the blank region.

266

267

#### 268 4. Probability of detection due to drizzle concentration

269

270 In the previous section, it was demonstrated that a radar with very small sampling volume ( $\sim cm^3$ )  
271 can plausibly achieve the detection of single drizzle droplets against a cloud background signal.

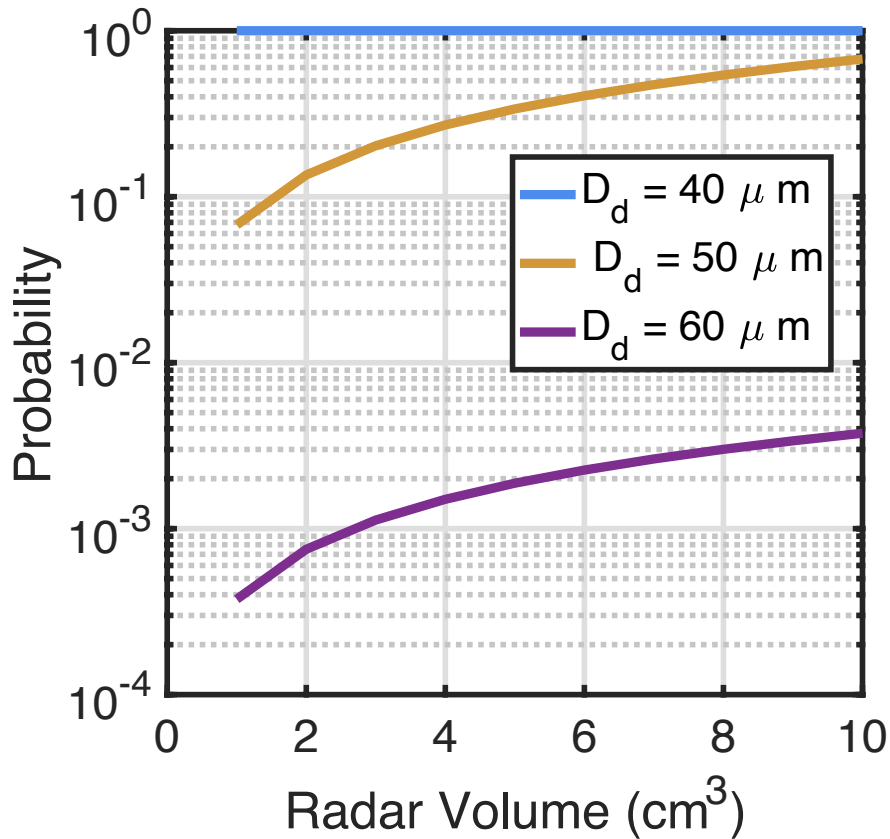
272 On the other hand, the smaller the radar volume, the lower the probability of a drizzle particle  
273 encountering the volume. To illustrate this trade-off scenario, we define the probability of drizzle  
274 occurrence in the radar volume ( $p(D_d)$ ) as:

275

$$276 \quad p(D_d) = \begin{cases} 1, & VN(D_d)\Delta D \geq 1 \\ VN(D_d), & VN(D_d)\Delta D < 1 \end{cases} \quad (9)$$

277

278 Specifically, the product of  $V$  and  $N(D_d)$  represents the expected number of drizzle drops in the  
279 radar volume. If the product is smaller than 1, it indicates the probability of the occurrence of  
280 drizzle particle in a given volume; while if the product is larger than 1, it means, statistically, at  
281 least one drizzle drop with a diameter of  $D_d$  exists in the radar volume, and thus we set  $p(D_d)=1$ .



283

284

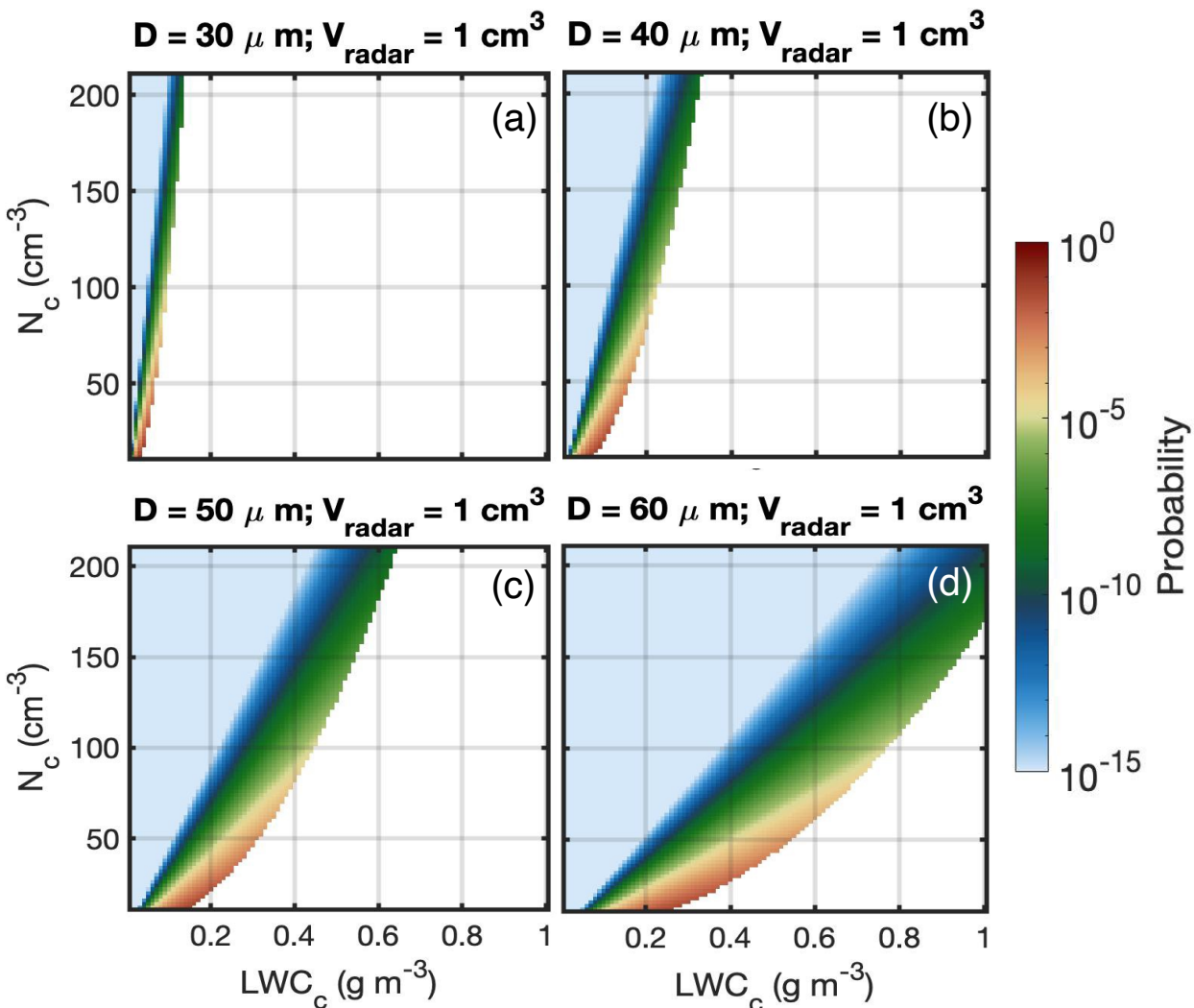
285 Figure 4: The probability of drizzle occurrence as a function of radar observational volume. The  
 286 blue, yellow, and purple lines indicate the drizzle particle with diameters of  $40 \mu m$ ,  $50 \mu m$ , and  $60$   
 287  $\mu m$ .

288

289 The probability of occurrence for three selected drizzle particles as a function of radar volume is  
 290 shown in Fig. 4. The  $N(D)$  in Eq. 9 is adapted from the size distribution described by Eq.6, with  
 291  $LWC_c$  and  $N_c$  set as  $0.5 g m^{-3}$  and  $50 cm^{-3}$ , respectively. For these conditions, drizzle droplets with  
 292 a diameter of  $40 \mu m$  have sufficiently high concentration to be on average always present in  
 293 volumes larger than  $1 cm^3$ . For drizzle droplets with a diameter of  $50 \mu m$  or  $60 \mu m$ , their  
 294 concentration is low enough that their probability of being found in a  $10 cm^3$  volume is on average  
 295 below 1. It is also noticed that the occurrence probability is strongly sensitive to the particle size:  
 296 the probability of drizzle with  $60 \mu m$  diameter occurring in the volume is almost two magnitudes  
 297 smaller than that for a particle with  $50 \mu m$  diameter. A smaller drizzle occurrence in the volume

298 indicates that a larger number of radar samples would be required to find one particle, leading to  
299 a longer observational time.

300  
301 The probability of a drizzle drop to be in the radar sampling volume or passing through the radar  
302 volume within a finite time period should be an important consideration for a practical  
303 measurement system. Fig. 5 shows the probability of the occurrence of drizzle particle under  
304 different chamber environments same as Fig. 3. The blank region in Fig. 5 indicates the  
305 corresponding SNR shown in Fig. 3 is lower than 0 (i.e., cannot be detected by the radar even they  
306 exist in the sampling volume). Generally, it is noticed that the probability of occurrence differs in  
307 various chamber environment for different droplet size: large droplets have lower occurrence  
308 probability under small LWC and high  $N$  conditions.



309 Figure 5: Drizzle occurrence probability under different LWC and  $N$  conditions for a  $1 \text{ cm}^3$  radar  
310 volume with particle diameter of (a)  $30 \mu\text{m}$ , (b)  $40 \mu\text{m}$ , (c)  $50 \mu\text{m}$ , and (d)  $60 \mu\text{m}$ . The blank region  
311 indicates that the associated SNR is smaller than 0 (Fig. 3).

312  
313 Comparison of Fig. 3 and Fig. 5 reveals that conditions that favor high radar SNR (i.e., larger drops  
314 or smaller radar sampling volume) are associated with a lower probability of occurrence of the  
315 drizzle droplet in the radar volume and subsequently increase the radar sampling time. For example,  
316 to detect a drizzle particle of  $50 \mu\text{m}$  diameter under the condition of  $\text{LWC}_c$  and  $N_c$  of  $0.3 \text{ g m}^{-3}$ ,  $90$   
317  $\text{cm}^{-3}$ , the particle occurrence probability is on the magnitude of  $10^{-8}$  (Fig. 5c) for SNR equals to 3  
318 (Fig. 3c). A 1 dB enhancement of SNR threshold would decrease the occurrence probability to  $10^{-$   
319  $^{11}$ . This implies that on average, a volume of air equal to  $10^{11}$  times the size of the radar sampling  
320 volume needs to be sampled before a drizzle droplet will be detected. Assuming an air mean flow  
321 within the cloud chamber of  $1 \text{ m s}^{-1}$ , this implies that a radar sampling volume with a typical  
322 dimension of  $1 \text{ cm}$  will be updated (through advection) 100 times per second. If the radar is  
323 sampling along 1000 range gates (i.e. assuming a chamber with height of 10 m), this suggests that  
324 the radar can sample a volume equal to  $10^5$  its radar sampling volume each second. To reach the  
325 average required sampling volume ( $10^{11}$ ), it will take  $10^6$  seconds or 11.5 days. This is an  
326 unrealistically long observational time. For practical application, we want to work with sampling  
327 configurations that will not require to sample more than  $10^9$  times the radar sampling volume ( $\sim 10$ s  
328 of minutes).

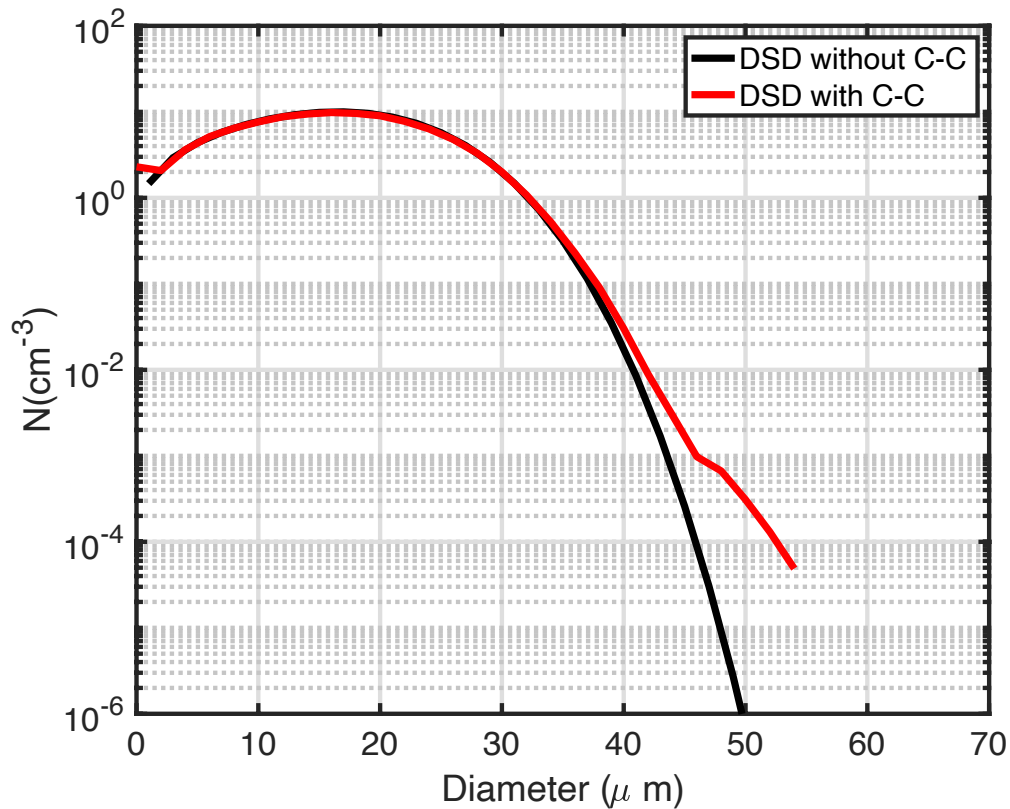
329  
330 Another factor to consider in estimating the probability of drizzle occurrence with a certain  
331 diameter in a specific volume is the realism of using Eq. 6 for describing the  $N(D)$  in a cloud  
332 chamber. Eq. 6 describes the cloud droplet distribution controlled by the condensation process  
333 alone, thus the results may underestimate the actual drizzle occurrence as condensation is  
334 inefficient to produce large drizzle particle. In nature or in a large convection cloud chamber, the  
335 C-C mechanism is expected to be a more efficient process to increase the size and concentration  
336 of drizzle droplets.

337  
338 Here we apply the ClusColl model to demonstrate that Fig. 4 and Fig. 5 may underestimate the  
339 drizzle occurrence probability with the collision-coalescence process being activate. ClusColl is a

340 simulation method for describing droplet motions and collisions in turbulent flows (Krueger and  
341 Kerstein, 2018). ClusColl simulates the movement of individual droplets in a vertical column due  
342 to turbulence and gravitational sedimentation. The unique capability of the ClusColl model is its  
343 capability to efficiently simulate the droplet collisions and coalescence process. Fig. 6 shows the  
344 simulated DSD with and without the collision-coalescence process for a 10-*m*-height cloud  
345 chamber and with cloud number concentration of  $100 \text{ cm}^{-3}$ . The temperature difference between  
346 top and bottom walls is  $40 \text{ }^\circ\text{C}$ . Noticeable differences can be identified at the right tail of the  
347 distribution, particularly for droplet diameter larger than  $40 \text{ }\mu\text{m}$ : more larger droplets are generated  
348 if the collision-coalescence process is active. The higher concentration of large drops results in a  
349 significantly shorter waiting time for detection compared to what was calculated for the  
350 condensation-only examples given in the earlier part. For instance, for the generated particle with  
351 diameter of  $50 \text{ }\mu\text{m}$ , the C-C process can generate number concentration more than 100 higher than  
352 the one without C-C process included. Reviewing the earlier estimation, to detect drizzle particle  
353 with diameter of  $50 \text{ }\mu\text{m}$  with SNR higher than 4, the required  $10^6 \text{ s}$  becomes  $10^4 \text{ s}$  which is  
354 approximately 3 hours, which is much more achievable for laboratory experiment. Thus, the  
355 estimation based on the condensation-only distribution (Eq. 6) is the most-conservative scenario.  
356 The actual radar measurement time would likely to be much shorter when the C-C process is  
357 activated.

358





360

361

362 Figure 6: DSD simulated from the ClusColl model with (red line) and without (black line) droplet  
 363 growth by collision-coalescence. In both cases, growth by condensation in a uniform  
 364 supersaturation field, and removal by size-dependent droplet sedimentation are calculated.  
 365 Therefore, the black line is described by the distribution given by Equation 6.

366

367

368

## 369 5. Evaluation from cloud chamber observations

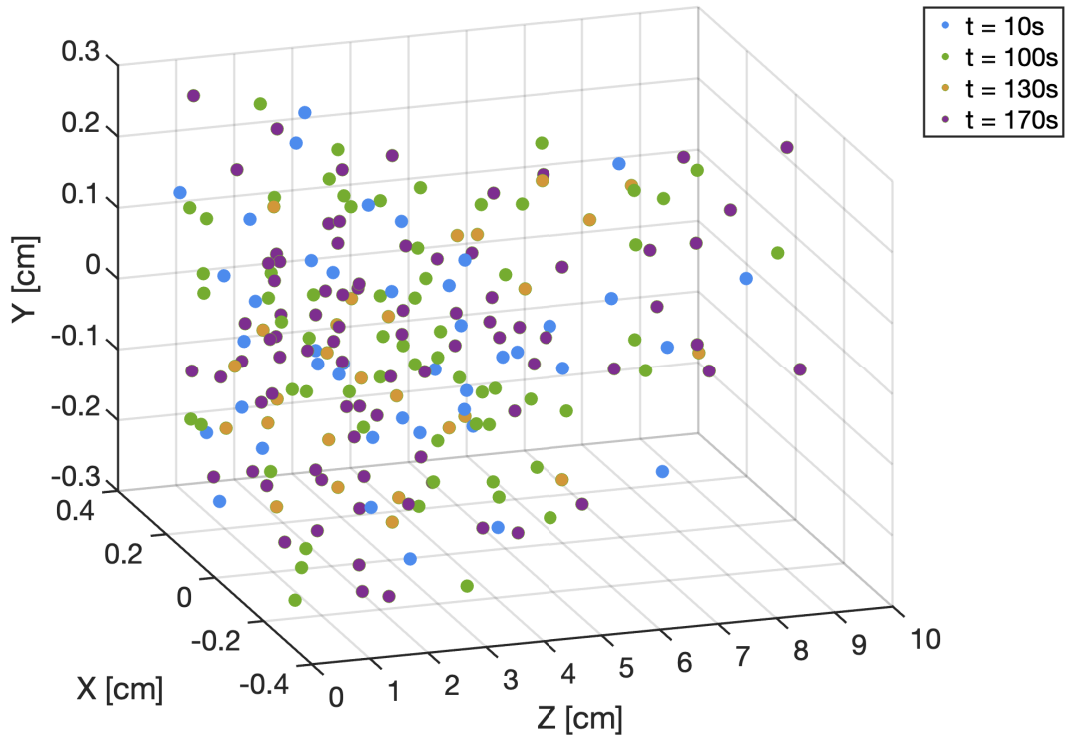
370

371 In a cloud chamber and in the real atmosphere, the DSD in the radar sampling volume is expected  
 372 to be time dependent due to turbulent fluctuations. To better quantify the particle backscattering  
 373 power and its fluctuation in a small volume, observations made in the Pi Chamber using a  
 374 holographic system (Holo-Pi) are used. Holo-Pi uses the principle of in-line digital holography to

375 measure the spatial distribution and sizes of cloud particles (Fugal and Shaw, 2009;Beals et al.,  
376 2015), and is specifically designed for the Pi-chamber environment (Desai et al., 2018). In contrast  
377 to the typical measurement strategy of single particle detections requiring time averaging, Holo-  
378 Pi captures instantaneous snapshots of all cloud droplets in the sample volume of  $3.6 \text{ cm}^3$  ( $0.6 \text{ cm}$   
379  $\times 0.6 \text{ cm} \times 10 \text{ cm}$ ) and is well suited to measure the temporal variations of cloud droplet  
380 populations within a sample volume similar to plausible radar sample volumes. The inability to  
381 resolve the smallest cloud droplets in the size distribution is not expected to be a significant  
382 limitation as the backscattering radar power is more sensitive to larger particle diameters. For the  
383 results presented here, cloud droplets are formed in the Pi Chamber by activation of size-selected  
384 sodium chloride aerosol particles (dry particle diameter  $\approx 130 \text{ nm}$ ) injected into a supersaturated  
385 turbulent flow sustained by an unstable temperature difference of 20 K. An illustration of the 3D  
386 view of the cloud droplets measured by Holo-Pi at different time instants in the Pi-chamber is  
387 shown in Fig. 7. The sample volume used for our calculations is limited to a vertical extent of 5  
388  $\text{cm}$  as particle detectability falls off beyond this point; this results in a total sample volume of  $1.8$   
389  $\text{cm}^3$ . The Holo-Pi system is set up to capture a hologram every 10 seconds during a 720-s period.  
390 For the optical configuration used here, the Holo-Pi has a lower size resolution of  $12 \mu\text{m}$   
391 throughout its sample volume.

392

393



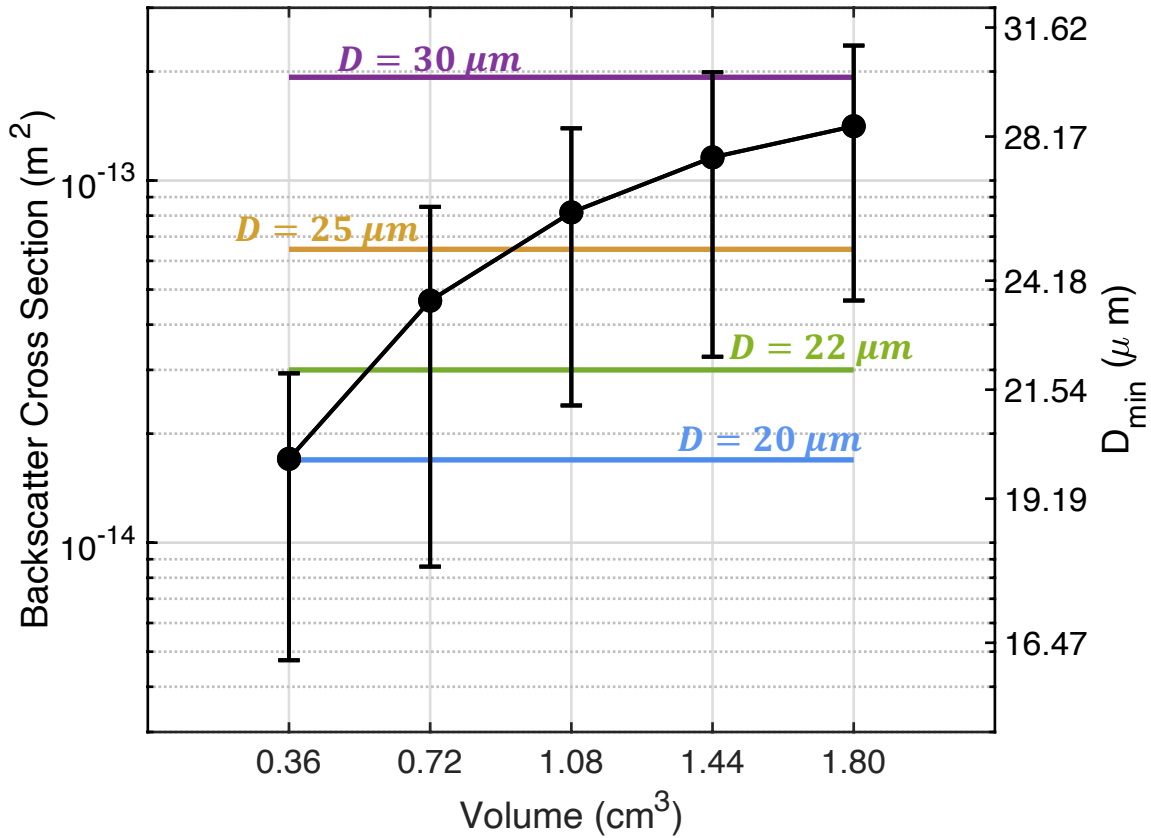
395

396 Figure 7: A 3D view of the particle locations observed by Holo-Pi in the Pi Chamber. Different  
 397 colors represent observations taken at different timesteps.

398

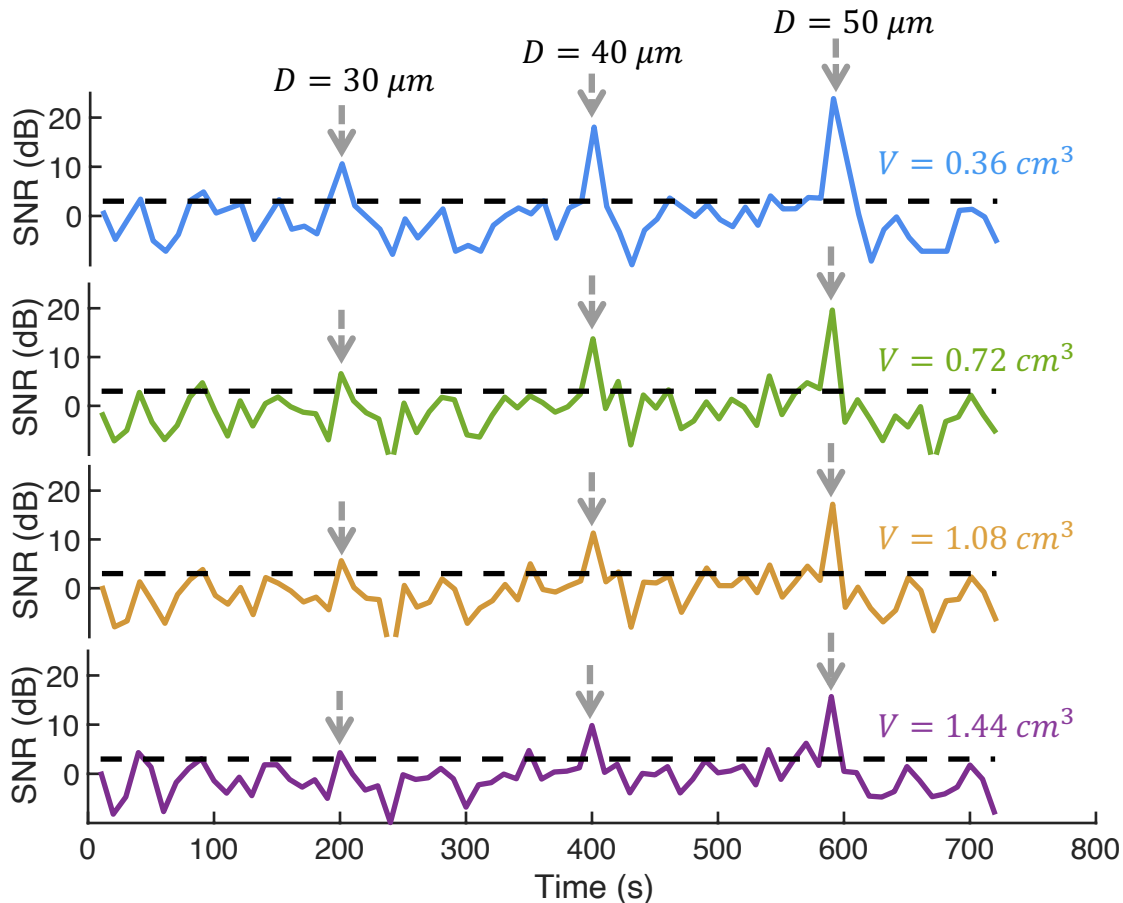
399 The Holo-Pi observational volume is divided into five sub volumes with the cross section of  $0.36$   
 400  $cm^2$  and the depth increasing from 1 to 5  $cm$  with an increment of 1  $cm$ , thus, corresponding to a  
 401 volume of 0.36, 0.72, 1.08, 1.44 and 1.8  $cm^3$ . Within each sub-volume at each time step, the total  
 402 backscattering cross section for the detected droplets is estimated using a THz radar with  
 403 wavelength of 0.44  $mm$ . The calculated radar backscattering cross section as a function of volume  
 404 size is shown in Fig. 8. Similar to the previous estimation, we see that the background power  
 405 increases with volume size due to the increment of cloud droplets. Importantly, the uncertainty  
 406 bars shown in Fig. 8 represent the standard deviation of the backscattering cross section during the  
 407 observational time, which indicates the background power fluctuations. We notice that the cloud  
 408 distribution in a small radar sampling volume is highly heterogeneous in time, and the magnitude  
 409 of the background fluctuation varies by approximately a factor of 10. In order to detect drizzle  
 410 drops, the backscattering power of the drizzle drop should be larger than the range of background

411 fluctuations. For example, a radar volume smaller than  $0.36 \text{ cm}^3$  should be utilized to detect a  
 412 droplet with a diameter larger than  $22 \mu\text{m}$ , and a radar sampling volume smaller than  $1 \text{ cm}^3$  is  
 413 needed to detect droplet with diameter larger than  $30 \mu\text{m}$  for this particular Pi Chamber experiment  
 414 set up.  
 415



416  
 417 Figure 8: Dots and uncertainty bars indicate the mean and standard deviation of the total  
 418 backscattering cross-section (with units of  $\text{m}^2$ ) of droplets measured in different volumes by Holo-  
 419 Pi during the observational period. The right axis and the horizontal lines represent the diameter  
 420 of a single drizzle drop with backscattering power equivalent to the background.

421 To further demonstrate the single drizzle detection concept using a small radar volume, a pseudo-  
 422 radar observation experiment is conducted based on the Holo-Pi measurements. The Holo-Pi  
 423 observational volume is divided into 4 sub-volumes indicated as different lines shown in Fig. 9. In  
 424 each volume, we consider the mean radar backscattering power from all cloud particles sampled  
 425 during the observational period as the background noise, and the power estimated at each time step  
 426 as the signal, such that the SNR as a function of observation time is estimated. To simulate the  
 427 drizzle occurring events, artificial drizzle droplets with diameter of  $30\ \mu\text{m}$ ,  $40\ \mu\text{m}$ ,  $50\ \mu\text{m}$  are  
 428 added to the volume at 200 s, 400 s, and 600 s, respectively, and the associated SNR is estimated.  
 429 Fig. 9 shows a clear SNR enhancement when the drizzle droplets are added. The signal  
 430 enhancement is more significant when using a small sampling volume and for larger drizzle drop  
 431 diameter, which is consistent with the theoretical estimation in Sec. 3. For instance, a drizzle drop  
 432 with a diameter of  $50\ \mu\text{m}$  can have a SNR of 23 dB with a volume of  $0.36\ \text{cm}^3$  while it has a SNR  
 433 of 15 dB with a volume of  $1.44\ \text{cm}^3$ . For a drizzle drop of  $30\ \mu\text{m}$ , the SNR with a volume of  $0.36$   
 434  $\text{cm}^3$  can reach to 10 dB, which is an adequate SNR value for radar detection, while with a volume



435 of  $1.44 \text{ cm}^3$ , the drizzle drop SNR is overwhelmed by background fluctuation and it is unable to  
436 be detected.

437

438 Figure 9: Simulated SNR of radar measurements during the Holo-Pi observational period using  
439 four sampling volumes:  $0.36 \text{ cm}^3$  (blue line),  $0.72 \text{ cm}^3$  (green line),  $1.08 \text{ cm}^3$  (yellow line) and  
440  $1.44 \text{ cm}^3$  (purple line). The grey arrows indicate an artificial drizzle particle is added at the  
441 indicated time step. The black dashed line indicates a SNR of 3, which is used as a threshold to  
442 distinguish the signal (drizzle) from the background (clouds) in Fig. 3.

443

## 444 6. Summary

445

446 Recent simulation results suggest that drizzle initiation could occur in a large convection-cloud  
447 chamber. Such a facility would provide measurements in a controlled environment that can  
448 advance our understanding of warm rain formation in clouds. One of the critical measurements in  
449 a large convection-cloud chamber is the detection of low-concentration drizzle droplets in the  
450 presence of numerous cloud droplets. Early in the drizzle initiation, those drizzle drops are rare  
451 and in-homogeneously distributed in the chamber, presenting a significant detection challenge for  
452 conventional in-situ probes. Here, the potential of a radar with ultra-fine sampling volume for  
453 drizzle detection is investigated. It was demonstrated that if the radar sampling volume becomes  
454 orders of magnitude smaller (e.g., several  $\text{cm}^3$ ), compared to those typically available in research  
455 radars ( $\sim 10^3$ - $10^6 \text{ m}^3$ ), isolated drizzle particles can be detected against the cloud background signal.  
456 This concept is based on the notion that the SNR of point targets (i.e., drizzle droplet) is  
457 independent of the radar sampling volume while the SNR of background (i.e., high concentration  
458 cloud droplets) scales with the sampling volume.

459

460 A theoretical DSD was adapted to represent the distribution of cloud droplets in a convection cloud  
461 chamber and to estimate properties of a detectable drizzle particle. It was shown that the minimum  
462 size of an isolated drizzle droplet that can be detected with such a radar depended on the radar  
463 sampling volume and the strength of the background signal (i.e., cloud droplets radar return), that  
464 in turn, depends on LWC and  $N_c$ . To minimize the false alarm drizzle detection, we require that  
465 the backscattering power from a drizzle particle should be larger than the backscattered power

466 contributed from the cloud particles ( $\text{SNR} > 1$ ). It is demonstrated that the application of a small  
467 radar volume can significantly enhance SNR under a given chamber environment. On the other  
468 hand, the smaller the radar sampling volume the lower the probability of an isolated drizzle droplet  
469 to be sampled. Thus, the determination of the radar volume for drizzle detection should account  
470 for the size of drizzle particle of interest, the environment conditions that favor drizzle initiation  
471 and the required observational time.

472  
473 In addition to analytical estimates, real observations from the MTU Pi convection-cloud chamber  
474 are used to demonstrate the single drizzle particle detection framework. The Holo-Pi system (Desai  
475 et al., 2018) is applied to provide detailed 3D imaging of the cloud particles in the cloud chamber,  
476 from which the fluctuations of the backscattering power in a small volume can be well estimated.  
477 Generally, the observational results are consistent with the theoretical estimation showing that the  
478 background power is decreased and the ability to detect drizzle particles is enhanced as radar  
479 sample volume is decreased. It is also noticed that the magnitude of the background fluctuation is  
480 comparable to the mean power, which indicate that the distribution of cloud droplets is highly  
481 inhomogeneous in the small volume. Thus, the power from a drizzle particle should at least  
482 dominate the background power fluctuation in order to be detected. With the cloud chamber  
483 environment from the experiment, drizzle particles with diameter larger than  $30 \mu\text{m}$  can be  
484 confidently detected using a radar sampling volume of  $1 \text{ cm}^3$  or lower.

485  
486 The key remaining question is the technological feasibility of building a radar that can operate  
487 within a box (large convection cloud chamber) and achieve the required ultra-fine range resolution.  
488 In fact, the effort of using “small” radar volumes for single particle detection has already been  
489 achieved in previous studies. For example, Schmidt et al. (2012) utilized a C-band radar with a  $14\text{-}$   
490  $\text{m}^3$  observational volume and successfully detected the trajectories of rain droplet with diameter  
491 down to  $0.5 \text{ mm}$ . In our case, the required radar sampling volume for drizzle detection is much  
492 smaller (with several  $\text{cm}^3$ ). Such ultra-fine range resolution can be achieved using a THz radar  
493 operating at 340 or 680 GHz that can support wide bandwidth waveforms and thus enable sub-  
494 centimeter range resolution (Cooper and Chattopadhyay, 2014). If the radar operates at a very high  
495 carrier frequency (THz) it can afford a very wide bandwidth for pulse modulation. In this case, the  
496 range resolution is not dictated by the pulse length but from the radar bandwidth (Cooper and

497 Chattopadhyay, 2014). The ultra-fine range resolution along with a reflector that minimizes the  
498 angular spread of the radar beam can result in radar sampling volumes of a few  $cm^3$ . Such radar  
499 imaging capabilities have been extensively used for security screening at airports, for example. In  
500 our context, additional complexity is introduced by the fact that this radar needs to operate in a  
501 chamber with typical dimension of  $\sim 10$  m. These technical design issues will be the focus of a  
502 follow-up paper study that will include real observations of drizzle droplets from a THz radar  
503 system.

504

505 To conclude, we outline three issues that will need to be properly addressed before a radar can be  
506 applied to the drizzle-detection problem in a cloud chamber:

507

508 1) Does the radar have enough sensitivity to detect a single drizzle particle? With the  
509 development of the THz technology, radar with centimeter resolution is achievable,  
510 however, the currently developed THz radars are mainly used to detect relatively hard  
511 targets that do not require ultra-high sensitivity. For the purpose of drizzle detection,  
512 however, the backscattering cross-section is on the order of  $10^{-13} m^2$ ; such lower receiving  
513 power would require the radar to have a much higher transmitting power or a larger antenna  
514 size. Fortunately, an advantage for the drizzle detection in a cloud chamber is that the radar  
515 detection range is only several meters depending on the size of the chamber. According to  
516 Eq. 1, radar receiving power is inversely proportional to the fourth power of the target  
517 distance. Thus, the small detection range may greatly relieve the demand for high  
518 sensitivity in the radar design. In addition, recent advancements in THz transmitters allow  
519 us to utilize higher power output transmitter ( $\sim 50$  to  $200 mW$ ) at THz frequencies such as  
520 340 GHz.

521

522 2) What are the appropriate radar sampling strategies for drizzle detection in a cloud chamber  
523 facility? Most of the cloud radars applied in the atmosphere are vertically pointing and can  
524 provide continuous observation at a given location along the radar beam. However as  
525 discussed in the paper, drizzle occurrence in the chamber is extremely rare and  
526 inhomogeneous in space and time. If the radar is vertically pointing, with the radar beam  
527 of several  $cm$  width, it may wait significant time for the radar to detect one drizzle drop.



528 Adding a scanning capability to the radar may provide a more efficient way to observe and  
529 detect drizzle in the cloud chamber.

530  
531 3) How to eliminate or reduce the degradation effect of the chamber environment on a radar  
532 signal? In particular, the cloud chamber is a humid environment with liquid particles  
533 continually falling towards the bottom. Accumulation of water on the radar antenna can  
534 also severally attenuate the transmitting power and degrade the radar detectability.  
535 Furthermore, the chamber walls and the in-situ instruments mounted inside would produce  
536 strong backscattering signals and pollute the backscattering signal from hydrometeors.  
537 Thus, the design of the radar should also account for radar instrument design and sampling  
538 strategies that minimize these noise sources so that the best possible detection capability  
539 can be achieved.

540  
541 In short, this paper demonstrates the conceptual feasibility of THz radars for rare drizzle detection  
542 in a laboratory context. Undoubtedly, the development of a high-resolution radar for drizzle  
543 detection in a cloud chamber needs close collaborations between cloud physics scientists and radar  
544 engineers moving forward.

545

546 **Competing interests.**

547 **P. K.** is an associate editor of AMT and the peer-review process was handled by an independent  
548 editor. The authors have no other competing interests to declare.

549

550 **Code/Data availability**

551 The codes and observations used to conduct all the analyses in this study are available upon  
552 request.

553

554

555 **Author contributions**

556 Zeen Zhu conceptualized and implemented the method, performed the analysis, produced the  
557 figures, and wrote the initial draft of the manuscript. Pavlos Kollias and Fan Yang contributed to  
558 the conceptualization and provide guidance on the analysis. Raymond A. Shaw and Alex B.  
559 Kostinski contributed to the simplified model described in Section 3.1. Steve Krueger provided  
560 the ClusColl model. Nithin Allwayin provided the Holo-Pi measurements from the Pi Chamber.  
561 All authors read the manuscript draft and contributed comments and manuscript editing.

562

563

564

565 **Acknowledgements**

566 Authors from Brookhaven National Laboratory were supported by the Office of Biological and  
567 Environmental Research in the Department of Energy, Office of Science, through the United States  
568 Department of Energy Contract No. DE-SC0012704. Authors from Michigan Technological  
569 University and from Stony Brook University (subaward 2105003Z8) acknowledge support from  
570 National Science Foundation award AGS-2133229. A. Kostinski, S. Krueger, R. Shaw, and F.  
571 Yang accomplished some of this work during a visit at the Kavli Institute for Theoretical Physics  
572 as part of the Multiphase Flows in Geophysics and the Environment program. KITP is supported  
573 in part by National Science Foundation under grant number PHY-1748958. We also want to thank  
574 Dr. Ken Cooper for the constructive discussion and for providing feedback to the manuscript.

575

576

577

578

579

580

581

582

583

584

585

586

587 **Reference**

588

589 Acquistapace, C., Kneifel, S., Löhnert, U., Kollias, P., Maahn, M., and Bauer-Pfundstein, M.:  
590 Optimizing observations of drizzle onset with millimeter-wavelength radars, *Atmospheric*  
591 *Measurement Techniques*, 10, 1783-1802, 2017.

592 Battan, L. J.: Radar observation of the atmosphere, 1973.

593 Beals, M. A., Fugal, J. P., Shaw, R. A., Lu, J., Spuler, S. M., and Stith, J. L.: Holographic  
594 measurements of inhomogeneous cloud mixing at the centimeter scale, *Science*, 350, 87-90,  
595 2015.

596 Beard, K. V., and Ochs III, H. T.: Warm-rain initiation: An overview of microphysical mechanisms,  
597 *Journal of Applied Meteorology and Climatology*, 32, 608-625, 1993.

598 Chandrakar, K., Cantrell, W., Kostinski, A., and Shaw, R.: Data supporting the paper "Dispersion  
599 aerosol indirect effect in turbulent clouds: laboratory measurements of effective radius", 2018.

600 Chandrakar, K. K., Saito, I., Yang, F., Cantrell, W., Gotoh, T., and Shaw, R. A.: Droplet size  
601 distributions in turbulent clouds: Experimental evaluation of theoretical distributions, *Quarterly*  
602 *Journal of the Royal Meteorological Society*, 146, 483-504, 2020.

603 Chang, K., Bench, J., Brege, M., Cantrell, W., Chandrakar, K., Ciochetto, D., Mazzoleni, C.,  
604 Mazzoleni, L., Niedermeier, D., and Shaw, R.: A laboratory facility to study gas-aerosol-cloud  
605 interactions in a turbulent environment: The  $\Pi$  chamber, *Bulletin of the American Meteorological*  
606 *Society*, 97, 2343-2358, 2016.

607 Comstock, K. K., Wood, R., Yuter, S. E., and Bretherton, C. S.: Reflectivity and rain rate in and  
608 below drizzling stratocumulus, *Quarterly Journal of the Royal Meteorological Society: A journal*  
609 *of the atmospheric sciences, applied meteorology and physical oceanography*, 130, 2891-2918,  
610 2004.

611 Cooper, K. B., and Chattopadhyay, G.: Submillimeter-wave radar: Solid-state system design and  
612 applications, *IEEE microwave magazine*, 15, 51-67, 2014.

613 Desai, N., Chandrakar, K. K., Chang, K., Cantrell, W., and Shaw, R.: Influence of microphysical  
614 variability on stochastic condensation in a turbulent laboratory cloud, *Journal of the Atmospheric*  
615 *Sciences*, 75, 189-201, 2018.

616 Falkovich, G., Stepanov, M. G., and Vucelja, M.: Rain initiation time in turbulent warm clouds,  
617 *Journal of applied meteorology and climatology*, 45, 591-599, 2006.

618 Feingold, G., Cotton, W. R., Kreidenweis, S. M., and Davis, J. T.: The impact of giant cloud  
619 condensation nuclei on drizzle formation in stratocumulus: Implications for cloud radiative  
620 properties, *Journal of the atmospheric sciences*, 56, 4100-4117, 1999.

621 Frisch, A., Fairall, C., and Snider, J.: Measurement of stratus cloud and drizzle parameters in ASTEX  
622 with a Ka-band Doppler radar and a microwave radiometer, *Journal of the Atmospheric Sciences*,  
623 52, 2788-2799, 1995.

624 Fugal, J., and Shaw, R.: Cloud particle size distributions measured with an airborne digital in-line  
625 holographic instrument, *Atmospheric Measurement Techniques*, 2, 259-271, 2009.

626 Johnson, D. B.: The role of giant and ultragiant aerosol particles in warm rain initiation, *Journal*  
627 *of Atmospheric Sciences*, 39, 448-460, 1982.

628 Kollias, Clothiaux, E., Miller, M., Albrecht, B., Stephens, G., and Ackerman, T.: Millimeter-  
629 wavelength radars: New frontier in atmospheric cloud and precipitation research, *Bulletin of the*  
630 *American Meteorological Society*, 88, 1608-1624, 2007.

631 Kollias, Remillard, J., Luke, E., and Szyrmer, W.: Cloud radar Doppler spectra in drizzling stratiform  
632 clouds: 1. Forward modeling and remote sensing applications, *Journal of Geophysical Research-*  
633 *Atmospheres*, 116, 10.1029/2010jd015237, 2011.

634 Kollias, Clothiaux, E. E., Ackerman, T. P., Albrecht, B. A., Widener, K. B., Moran, K. P., Luke, E. P.,  
635 Johnson, K. L., Bharadwaj, N., and Mead, J. B.: Development and applications of ARM millimeter-  
636 wavelength cloud radars, *Meteorological Monographs*, 57, 17.11-17.19, 2016.

637 Kostinski, A. B., and Shaw, R. A.: Fluctuations and luck in droplet growth by coalescence, *Bulletin*  
638 *of the American Meteorological Society*, 86, 235-244, 2005.

639 Krueger, S. K., and Kerstein, A. R.: An economical model for simulating turbulence enhancement  
640 of droplet collisions and coalescence, *Journal of Advances in Modeling Earth Systems*, 10, 1858-  
641 1881, 2018.

642 Krueger, S. K.: Equilibrium droplet size distributions in a turbulent cloud chamber with uniform  
643 supersaturation, 2020.

644 Liu, Y., Geerts, B., Miller, M., Daum, P., and McGraw, R.: Threshold radar reflectivity for drizzling  
645 clouds, *Geophysical research letters*, 35, 2008.

646 Pinsky, and Khain, A.: Turbulence effects on droplet growth and size distribution in clouds—A  
647 review, *Journal of aerosol science*, 28, 1177-1214, 1997.

648 Pruppacher, H. R., and Klett, J. D.: *Microphysics of Clouds and Precipitation: Reprinted 1980*,  
649 Springer Science & Business Media, 2012.

650 Saito, I., Gotoh, T., and Watanabe, T.: Broadening of cloud droplet size distributions by  
651 condensation in turbulence, *Journal of the Meteorological Society of Japan. Ser. II*, 2019.

652 Schmidt, J. M., Flatau, P. J., Harasti, P. R., Yates, R. D., Littleton, R., Pritchard, M. S., Fischer, J. M.,  
653 Fischer, E. J., Kohri, W. J., and Vetter, J. R.: Radar observations of individual rain drops in the free  
654 atmosphere, *Proceedings of the National Academy of Sciences*, 109, 9293-9298, 2012.

655 Shaw, R. A.: Particle-turbulence interactions in atmospheric clouds, *Annual Review of Fluid*  
656 *Mechanics*, 35, 183-227, 2003.

657 Shaw, R. A., Cantrell, W., Chen, S., Chuang, P., Donahue, N., Feingold, G., Kollias, P., Korolev, A.,  
658 Kreidenweis, S., and Krueger, S.: Cloud–aerosol–turbulence interactions: Science priorities and  
659 concepts for a large-scale laboratory facility, *Bulletin of the American Meteorological Society*,  
660 101, E1026-E1035, 2020.

661 Shaw, R. A., Thomas, S., Prabhakaran, P., Cantrell, W., Ovchinnikov, M., and Yang, F.: Fast and  
662 slow microphysics regimes in a minimalist model of cloudy Rayleigh-Bénard convection,  
663 *Physical Review Research*, 5, 043018, 10.1103/PhysRevResearch.5.043018, 2023.

664 Thomas, S., Yang, F., Ovchinnikov, M., Cantrell, W., and Shaw, R. A.: Scaling of turbulence and  
665 microphysics in a convection–cloud chamber of varying height, *Journal of Advances in Modeling*  
666 *Earth Systems*, 15, e2022MS003304, 2023.

667 Wood: Stratocumulus Clouds, *Monthly Weather Review*, 140, 2373-2423, 10.1175/mwr-d-11-  
668 00121.1, 2012.

669 Yau, M. K., and Rogers, R. R.: *A short course in cloud physics*, Elsevier, 1996.

670 Zhu, Z., Kollias, P., Luke, E., and Yang, F.: New insights on the prevalence of drizzle in marine  
671 stratocumulus clouds based on a machine learning algorithm applied to radar Doppler spectra,  
672 Atmospheric Chemistry and Physics, 22, 7405-7416, 2022.  
673